ACS APPLIED MATERIALS & INTERFACES

Research Article

www.acsami.org

Homogeneous Lithium Electrodeposition with Pyrrolidinium-Based Ionic Liquid Electrolytes

Lorenzo Grande,[†,‡,§] Jan von Zamory,[†,‡,§] Stephan L. Koch,[†,‡,§] Julian Kalhoff,[§] Elie Paillard,*[,†,‡,§] and Stefano Passerini*[,†,‡,§]

[†]Helmholtz-Institut Ulm (HIU) Electrochemistry I, Albert-Einstein-Allee 11, 89081 Ulm, Germany

[‡]Karlsruhe Institute of Technology (KIT), P.O. Box 3640, 76021 Karlsruhe, Germany

[§]Institute of Physical Chemistry, University of Münster, Corrensstraße 28−30, 48149 Münster, Germany

ABSTRACT: In this study, we report on the electroplating and stripping of lithium in two ionic liquid (IL) based electrolytes, namely *N*-butyl-*N*-methylpyrrolidinium bis(fluorosulfonyl) imide ($Pyr_{14}FSI$) and *N*-butyl-*N*-methylpyrrolidinium bis(trifluoromethanesulfonyl)imide ($Pyr_{14}TFSI$), and mixtures thereof, both on nickel and lithium electrodes. An improved method to evaluate the Li cycling efficiency confirmed that homogeneous electroplating (and stripping) of Li is possible with TFSI-based ILs. Moreover, the presence of native surface features on lithium, directly observable via scanning electron microscope imaging, was used to demonstrate the enhanced electrolyte interphase (SEI)-forming ability, that is, fast cathodic reactivity of this class of electrolytes and the suppressed dendrite growth. Finally, the induced inhomogeneous deposition enabled us to witness the SEI cracking and revealed previously unreported bundled Li fibers below the pre-existing SEI and nonrod-shaped protuberances resulting from Li extrusion.

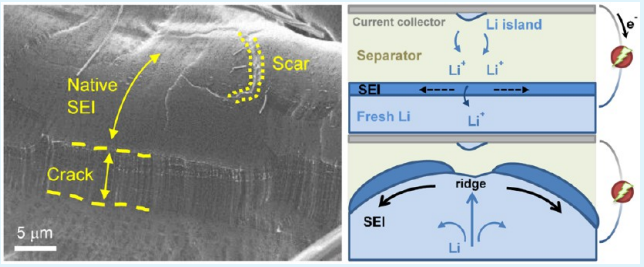

KEYWORDS: *lithium metal, dendrites, ionic liquids, SEI, energy storage, nickel*

1. INTRODUCTION

Electrochemical energy storage has established itself as an essential technology in several applications, be it intermittent renewable energy sources, laptops, smartphones ,or electric vehicles. Li-ion batteries have quickly gained the lion's share of the market thanks to their high specific energy. However, the "rocking chair" concept faces an intrinsic theoretical limitation of 250−300 W h kg^{-1}, mostly because of restrictions related to the cathode's maximum specific capacity and voltage.[1−3] Resorting to new battery chemistries is therefore vital if higher energy densities are to be reached. Lithium has long been proposed as a good anode material for Li-metal, Li/S, and Li/O_2 batteries.[2] It sports a high specific capacity (3861 mA h g^{-1}) and a very negative potential (−3.05 V vs SHE), but has found only limited commercial applications in secondary batteries due to its high reactivity and tendency to form short circuits. The first phenomenon leads, in aprotic electrolytes, to the formation of an electronically insulating (but ionically conductive) passivation layer on top of lithium every time a fresh surface is exposed to the electrolyte. This film, which has been dubbed the solid−electrolyte interphase (SEI),[4] consists of a mix of organic and inorganic insoluble compounds that result from native species and electrolyte decomposition products. It is an unavoidable phenomenon and generally regarded as a protective layer. Undesired side reactions can, however, still take place during cell operation, leading to a low Coulombic efficiency and irreversible capacity loss. The situation is further exacerbated by inhomogeneous Li deposition, which can induce short circuits through what are commonly known as dendrites, whose uncontrolled growth causes the perforation of the separator (or polymer electrolyte) and internal cell failure.[5]

Several models have been proposed to explain the mechanisms of dendrite onset, growth, or both, among which it is worth noting those by Chalzaviel et al.[6−8] and Yamaki et al.[9] The first one predicts that nucleation and growth of dendrites initiate when the applied current density hits the limiting value i_{lim} and triggers the depletion of Li^+ ions at the surface of the metal, causing a large, localized electric field to appear at the interface. Dendrite growth can occur, however, even below i_{lim}, due to small interelectrode distance and surface defects that are responsible for a localized increase in current density.[10] Ways to circumvent the detrimental effect of defects have been devised, such as applying an external pressure,[11] pulse charging,[12] using composite polymer electrolytes,[13] ionic liquids (IL),[14,15] block copolymers,[16] and protective films/additives,[17−22] but surface imperfections remain intrinsic and unavoidable. Yamaki et al. stressed the importance of such defects by describing the conditions under which dendrites can grow. According to them, lithium deposition takes place underneath the SEI, until stress on its surface leads to a disruption of the texture and to the extrusion

Received: January 8, 2015
Accepted: February 25, 2015
Published: February 25, 2015

DOI: 10.1021/acsami.5b00209
ACS Appl. Mater. Interfaces 2015, 7, 5950−5958

of lithium from these sites. Deposition can continue at the base of these whisker-like structures until Li^+ transport is sufficiently hindered. At this point, deposition starts to take place on the tip and at the whiskers' kink sites, which are rich in lattice defects. During the reverse process, such whiskers dissolve at the base (where the SEI is fresher and less resistive), ultimately causing the physical detachment of the outgrowths from the substrate.[9] Finally, according to the authors, a higher current during stripping is beneficial for the cycle life because it promotes the dissolution of lithium at the tip and kink sites rather than from the base. However, the assumptions of Yamaki's model are rather broad and neglect both lithium's rheological properties and the elasticity of the SEI, which Monroe and Newman[23] have taken into account in an alternative explanation based on Li^+ mass transport in solution and surface tension. More recently, Kramer et al. observed a mixed kink−tip−base growth behavior via in situ optical microscopy with carbonate-based electrolytes.[24,25] They showed the role played by the SEI shell present on lithium whiskers, which prevents dendrite shortening during lithium dissolution and favors a thinning mechanism, instead. Furthermore, they also stressed the importance of defect sites (be it SEI irregularities or lattice defects) and ionic mass transport in triggering needle-like dendrites, in accordance with other recent observations.[24,26,27] A uniform, low resistance and elastic SEI is paramount to ensure good lithium deposition,[28] and ionic liquids are among the proposed solutions to form an interphase with such characteristics and mitigate side effects. Basile et al. studied the cyclability of lithium after chemical interaction with *N*-propyl-*N*-methylpyrrolidinium bis(fluorosulfonyl)imide ($Pyr_{13}FSI$) and lithium tetrafluoroborate ($LiBF_4$) as salt. They followed the changes in morphology through scanning electron microscopy (SEM) and recorded cauliflower-like shapes appearing on the surface of lithium after 18 days of reaction with the electrolyte, which, however, did not impact the cyclability.[20] A smooth surface after extensive cycling was recorded by the same group using lithium bis(fluorosulfonyl)imide (LiFSI) as salt in the same IL.[29] In both works, a 12 h rest period was fixed before each lithium plating/stripping tests, which, in the authors' view, allowed the FSI^- anion to react and build a stable SEI on the metal surface, thanks to the cleavage of the S−F bond in FSI^-.[30,31] Our group recently showed that lithium bis(trifluoromethanesulfonyl)imide (LiTFSI) in *N*-butyl-*N*-methylpyrrolidinium bis(trifluoromethanesulfonyl)imide ($Pyr_{14}TFSI$) also contributes to an enhancement in cyclability if a rest period of 1 week is provided to the cell,[32] in spite of the higher strength of the anion's C−F bond. The adoption of a $TFSI^-$ anion allows to extend the IL's electrochemical stability window on the cathodic side,[33,34] thereby increasing its tolerance to lithium metal and inhibiting electrolyte degradation during cycling.

In this study, we analyzed the interplay between ionic liquid mixtures containing these two anions in terms of lithium nucleation and deposition on nickel and addressed the efficiency determination of Li metal cycling when an initial homogeneous plating cannot be reached. Finally, we report unique observations of the morphological changes underneath the SEI during Li deposition onto Li foil.

2. EXPERIMENTAL SECTION

2.1. Materials Used. Lithium foil (50 μm, 99.999%) was obtained from Rockwood Lithium GmbH, and stored in a dry room (relative humidity (RH) <0.1% at 20 °C) together with all the other chemicals. $Pyr_{14}TFSI$ and $Pyr_{14}FSI$ were synthesized and purified according to a well-established procedure[35] and subsequently vacuum-dried at 90 °C for at least 24 h with a turbo molecular pump ($P < 10^{-7}$ mbar). This step leads to colorless ILs exhibiting a water content below 2 ppm, measured via coulometric Karl Fischer titration (C30, Mettler Toledo). LiTFSI (99.9%, battery grade, 3M) was dried at 120 °C under vacuum for at least 24 h before use. The electrolytes were mixed according to different molar ratios (listed in Table 1) and further dried under turbo molecular vacuum at 70 °C for 24 h.

Table 1. Molar Ratios of the Electrolyte Mixtures Analyzed in This Study

sample name	FSI^- molar ratio	$TFSI^-$ molar ratio	Pyr_{14}^+ molar ratio	Li^+ molar ratio
0:1		0.5	0.45	0.05
3:7	0.15	0.35	0.45	0.05
1:1	0.25	0.25	0.45	0.05
7:3	0.35	0.15	0.45	0.05
9:1	0.45	0.05	0.45	0.05

Whatman GF-F glass fiber separators (GE Healthcare UK, Ltd.) were dried at 120 °C for at least 24 h prior to usage. Ni foil strips with a 20 μm thickness were used both as current collector and as working electrode in the plating/stripping tests.

2.2. Cell Assembly and Characterization. All cells were assembled inside the dry room according to a procedure already described.[32] The active area of the cells thus fabricated was ca. 1 cm^2. All Li/Li cells were assembled within a few hours to ensure similar initial SEI properties, then placed in an MK53 climatic chamber (Binder GmbH) with a $\Delta T = \pm 0.1$ °C at either 20, 40, or 60 °C.

The interfacial resistance evolution was monitored via electrochemical impedance using a Solartron 1287 potentiostat/galvanostat coupled to a Solartron 1260 frequency response analyzer (Solartron Analytical, Ltd.). The obtained spectra, which spanned a range of 65 kHz to 10 mHz, were then fitted using an equivalent circuit described in our previous publication.[32]

Galvanostatic tests were performed on a battery cycler (S4000, Maccor, Inc.) at 0.1 mA cm^{-2} with cutoff voltages of 0.5 and −0.5 V. The current was reversed every 60 min for the plating/stripping tests, while it was kept constant during the continuous plating experiments. Thermal equilibration of the cells was ensured by inserting a 12 h rest step before the beginning of each test.

The morphology of the lithium and Ni foil electrodes was analyzed via an AURIGA EVO MA 10 scanning electron microscopy (Zeiss) and a Tabletop Microscope TM-1000 (Hitachi). Lithium electrodes were rinsed three times with dimethyl carbonate (99%, Sigma-Aldrich) to remove IL traces and then dried under vacuum.

X-ray photoelectron spectroscopy (XPS) on lithium electrodes was carried out using an Axis Ultra HAS spectroscope (KRATOS) equipped with a monochromatic Al Kα source at 10 mA and 12 kV. A pass energy of 20 eV was employed for the measurements, and sample charging was compensated with a charge neutralizer. The analysis area on the sample surface was about 300 × 700 μm. The electrodes were transferred to the antechamber under argon atmosphere to avoid contact with oxygen and moisture. For the comparative evaluation of the obtained spectra, energy indication and component fitting were calibrated according to the peak for amorphous carbon in the C 1s spectra, due to its characteristic binding energy of 285 eV.

3. RESULTS

3.1. Plating on Ni Electrode. Plating/stripping of Li is a useful tool to estimate the compatibility between lithium metal and a given electrolyte.[36] To estimate the efficiency of the process, a fixed amount of lithium is plated on a metal electrode and then a fraction of it is shuttled back and forth,

DOI: 10.1021/acsami.5b00209
ACS Appl. Mater. Interfaces 2015, 7, 5950−5958

which allows calculating the average efficiency through the equation:

$$\text{Eff} = 1 - \frac{Q_p - Q_c}{nQ_c}$$

where Q_p is the amount of charge plated during the first cycle, n the number of cycles, and Q_c the charge that is plated/stripped at each cycle. In an asymmetrical cell (i.e., where the working electrode is not lithium metal), Q_p is generally chosen as 10 times Q_c, while in a symmetrical configuration (Li/Li) this value is predetermined by the Li reservoir already present in the electrode. Because the Li reservoir of symmetrical cells is generally 1 or 2 orders of magnitude larger than needed, $(Q_p - Q_c)$ can, in these cases, be approximated to Q_p.[32] The number of cycles that can be achieved reversibly gives an indication of the uniformity of the lithium deposit and the amount of parasitic reactions. Our attempts at estimating the average plating/stripping efficiency with Li/Ni cells failed and only led to limited and irreproducible cycling. An SEM investigation of the Ni electrode (portrayed in Figure 1a) revealed the presence of spherical dendrites on its surface, with an accumulation toward the metal's edges, suggesting a localized nucleation on surface irregularities.

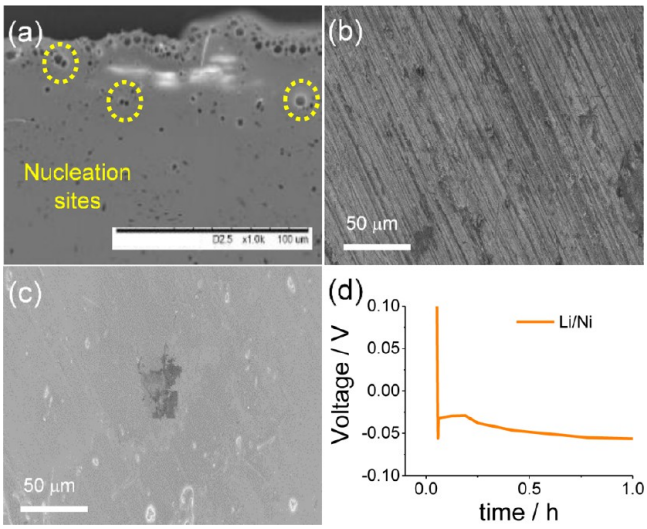

Figure 1. SEM images of (a) a Ni electrode after 10 h plating from the 0:1 electrolyte (the circled dark dots evidence the dendrites), (b) a pristine Ni foil, and (c) Li homogeneously deposited on Ni foil using a 9:1 electrolyte. (d) Plating potential of a Li/Ni cell showing the characteristic spike at around −50 mV associated with the nucleation of Li crystals onto the Ni surface.

Thus, it seems clear that Ni foil induces fast dendrite growth, which can easily be explained by the intense current density reached locally at the few nucleation points, in accordance with Chazalviel's model.[6−8] This observation is in contradiction with the long-term cycling obtained using Pyr_{14}TFSI in Li/Li cells,[32] as well as other observations that show the positive effect of TFSI-based ionic liquids in suppressing dendrite growth.[14] However, it agrees with the results reported by Howlett et al., who met similar difficulties on a Cu electrode,[37] and Wibowo, who failed to obtain a reversible plating/stripping on a Ni microelectrode, supposedly due to the poor SEI-forming ability of Pyr_{14}TFSI on the metal.[38] Only through the addition of vinylene carbonate to a series of ILs, including Pyr_{14}TFSI, were Matsumoto et al.[19] able to establish a uniform lithium electrodeposition regime on a Ni substrate, thereby effectively suppressing dendrites. Unlike Li metal, that is already passivated, nonlithiated materials require the formation of an SEI during the first cycle prior to other reduction processes (insertion, plating, or degradation of electrolyte components), to provide with Li nucleation sites and allow for a homogeneous transport to the electrode. The same problems were not observed when using an FSI-rich electrolyte (Figure 1c), hinting to the conclusion that FSI^- and $TFSI^-$ react differently at the Ni electrode. The reason lies in the narrower electrochemical stability of the former anion, resulting in the fast formation of an SEI, as it has already been shown on graphite[39] and Ni,[36,40] that would act as a good nucleation substrate. The stabilization of the solid-electrolyte interphase is therefore crucial, as we pointed out in a previous publication,[32] and as Figure 1a shows, it does not take place at high potentials for Pyr_{14}TFSI.

3.2. Influence of the FSI^-/$TFSI^-$ Ratio on SEI Evolution and Plating on Ni. The influence of the FSI/TFSI ratio on the SEI formation was investigated using Li/Li cells stored at different temperatures. Analogous blends have already been reported with regards to the synergistic effect of the two anions on the overall physicochemical properties, with FSI^- providing the final mixture with lower viscosity and higher ionic conductivity, and $TFSI^-$ extending the electrochemical stability window.[41,42] Figure 2 shows the evolution of the SEI resistance (R_{SEI}) for different ratios at three different temperatures. At 20 °C, a surge in SEI resistance is observed for all samples, with a more marked increase for electrolytes that have a higher TFSI ratio. At 40 °C, the situation differs notably, with the R_{SEI} of samples 0:1 and 3:7 first reaching a peak and then dropping considerably. The time scale within which this maximum is reached is shorter for 3:7 than 0:1, indicating faster reaction kinetics promoted by the presence of the FSI^- anion.

Cells containing higher FSI molar fractions, on the other hand, reach stable and similar values (ca. 40 Ω cm^2) within 1 day. At 60 °C, the cell containing the 0:1 mixture exhibits a high starting value, followed by a considerable drop in R_{SEI}; this behavior suggests that temperature speeds up the reaction kinetics behind the SEI formation. When FSI^- is added to the blends, the situation becomes mixed, with the only common feature being the stabilization between 30 and 40 Ω cm^2 after 1 week. While the complexity of the factors involved (such as the presence of an initial SEI, its wetting by the electrolyte, and the solubility of reduction products) makes the complete understanding of these evolutions difficult, it is clear that at 20 and 40 °C, the presence of a high fraction of FSI^- accelerates the evolution of a stable interface. This effect vanishes at 60 °C, when either anion seems to react rather quickly with Li.

The influence of the FSI^- anion toward plating on Ni was also investigated. SEM images obtained after a 10 h plating at 0.1 mA cm^{-2} reveal a lithium morphology which evolves from one close to the 0:1 electrolyte, with the Ni electrode covered by discrete deposits of Li (Figure 3a,b), to a situation close to the 1:0 morphology, where the Ni electrode is covered by a rather homogeneous Li layer (Figure 3c). However, in all the analyzed blends it was still not possible to perform stripping/plating, most likely because of the electrochemical inactivation of the deposits that leads to high overpotentials and ultimately low Coulombic efficiency.

3.3. Alternative Efficiency Estimation Method. The impossibility to obtain a good first plating of Li on Ni restricts efficiency determination tests to Li/Li configurations only. This obviously affects the experiments' time scale, which can require up to 8 months for a single measurement.[32] For this reason, an

DOI: 10.1021/acsami.5b00209
ACS Appl. Mater. Interfaces 2015, 7, 5950−5958

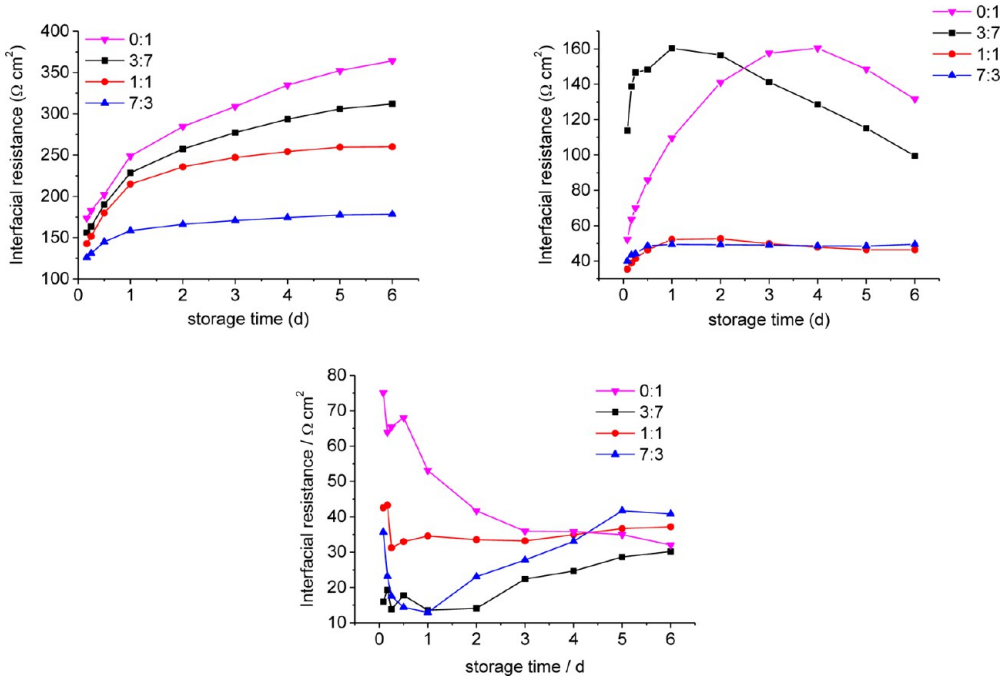

Figure 2. Interfacial resistance evolution in Li/Li pouch cells at (a) 20, (b) 40, and (c) 60 °C, for electrolyte mixtures with the following $FSI^-/TFSI^-$ molar ratios: 0:1, 3:7, 1:1, 7:3.

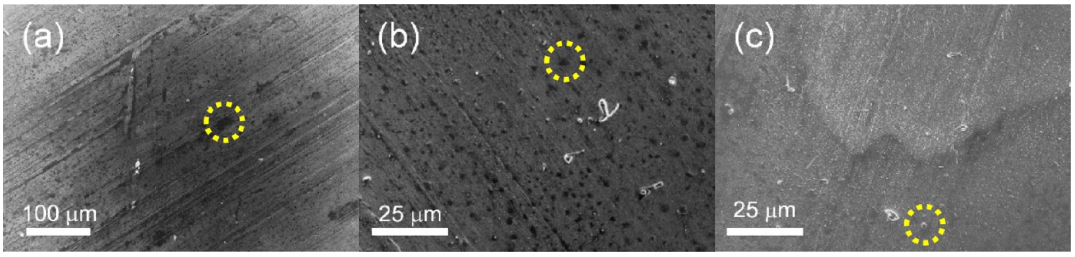

Figure 3. SEM images of lithium deposits on nickel in (a) 3:7, (b) 1:1, and (c) 7:3 $FSI^-/TFSI^-$ electrolyte mixtures. Microsized round features are found on the surface after Li deposition (circled in yellow).

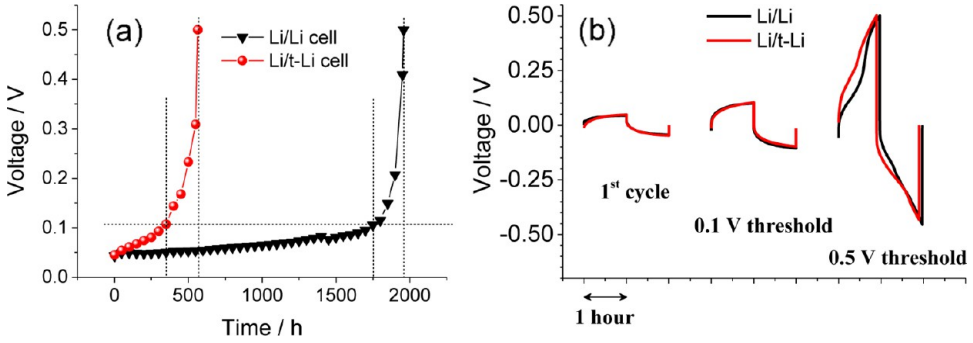

Figure 4. (a) Voltage profile corresponding to (black) a symmetrical Li/Li cell and (red) a symmetrical cell that was subjected to 90% stripping of one of its electrodes, here indicated as Li/t-Li; (b) voltage profiles of selected cycles as indicated on the graph. T = 40 °C, i = 0.1 mA cm^{-2}.

inverse approach was adopted: a symmetrical Li/0:1/Li cell made of two 50 μm thick Li electrodes (equivalent to ca. 10.32 mA h cm^{-2} each) was assembled and, prior to cycling, 90% of the Li was stripped from one of the two electrodes so that only 1 mA h cm^{-2} remained on the Ni current collector. Because plating of Li on Li with TFSI-based electrolytes is possible, this enabled us to perform the efficiency determination tests, using the standard value of $Q_p = 10\ Q_c$. The Li/thinned-Li cells thus manufactured were labeled as "Li/t-Li", to distinguish them from conventional stripping/plating tests.[36]

Figure 4a shows the cycling results obtained with the pristine (50 μm Li foil) and stripped (electrochemically thinned, 5 μm) electrodes. The two electrodes exhibit an identical final increase in overvoltage once the 100 mV overvoltage threshold is stepped over. This can be attributed to the thickening of the SEI with time and the subsequent increase in mass transport limitation for Li^+,

DOI: 10.1021/acsami.5b00209
ACS Appl. Mater. Interfaces 2015, 7, 5950−5958

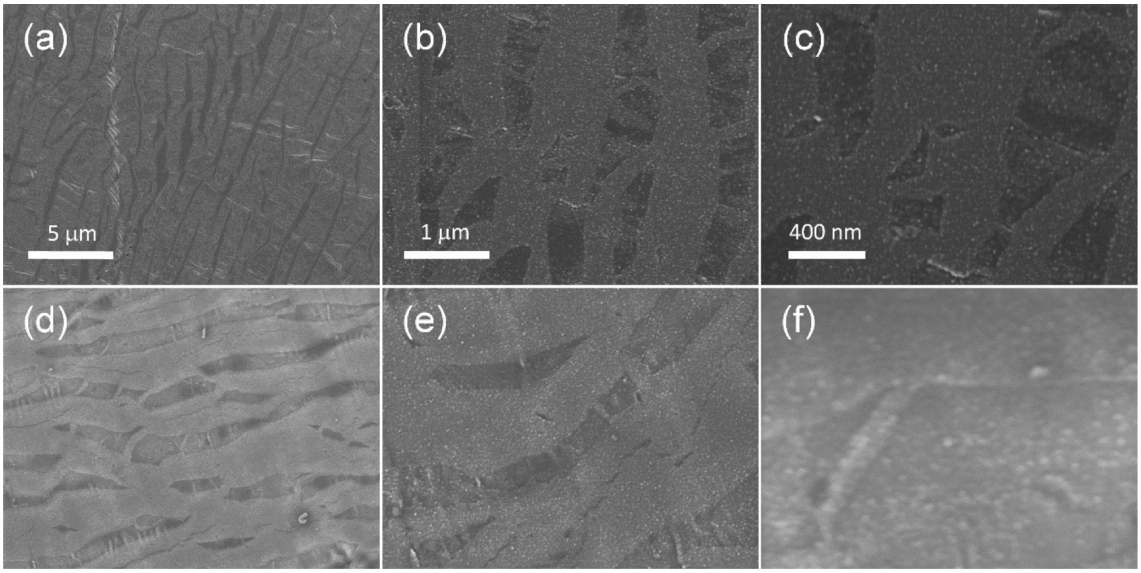

Figure 5. Different magnifications of (a–c) fresh Li foil and (d–f) Li foil taken from a Li/IL/Li pouch cell.

and it indicates the complete equivalence of the two measures, as confirmed by the first cycle voltage profiles depicted in Figure 4b. Upon cycling, both cells reached the 100 mV threshold. Their voltage profiles overlap quite well, although the time (i.e., the number of cycles) required for reaching such a threshold was about 4 times longer in the case of the Li/Li cell. However, the voltage profiles of the two cells differ substantially when the upper 500 mV boundary is reached (Figure 4b, third voltage profile). The Li/Li profile shows two plateaus, a phenomenon that is ascribable to either the buildup of a thick SEI over the surface of lithium or to the clogging of the SEI's Li^+ diffusion channels.[32] The same is not observed for the Li/t-Li cell, probably because the Li electrodes in the cell are given less time to accumulate decomposition products. Despite this difference, the two protocols can be regarded as equivalent. The values of efficiency obtained were 98.41% for the Li/t-Li cell, versus 94.77% for the symmetrical equivalent, also in line with our previous observations.[32] It must be stated that these values represent an underestimate of the real performance, because Li cycling can still occur, albeit at the cost of a high overpotential. The results show that fast efficiency determination tests for lithium electrodes are possible with electrolytes that do not allow a uniform nucleation on different substrates other than Li, while curbing down the overall measuring time by 70%.

3.4. Morphology of Li Foil during Electrodeposition. A question that arises at this point is whether the 90% of lithium initially deposited on the Li anode forms an irregular layer, as this would negatively bias the test, with special reference to the shorter measuring time recorded with the Li/t-Li cell. With this scope in mind, two pieces of Li foil were observed in this way, the first being a fresh, unused, unwashed strip of Li foil, the second a strip taken from an assembled (uncycled) pouch cell after rinsing with DMC. As shown in Figure 5a–c, groove-like features are present on the surface of the pristine Li foil. These most likely derive from the extrusion/calendering step utilized in the industrial process and are found homogeneously throughout the foil.

The sample obtained from the pouch cell appears identical (Figure 5d—f), despite having been in contact with the separator, the electrolyte, and the rinsing solvent. In addition, the vacuum under which pouch cells are fabricated does not seem to have either flattened or damaged the grooves observed on the sample. This finding provides a baseline morphology of the metal's surface that can be monitored upon deposition/dissolution to assess the uniformity of our Li plating/stripping and the mechanical integrity of the SEI. A chart depicting the typical chronopotentiogram recorded while plating on Li is shown in Figure 6. The plating overvoltage ΔV remains constant

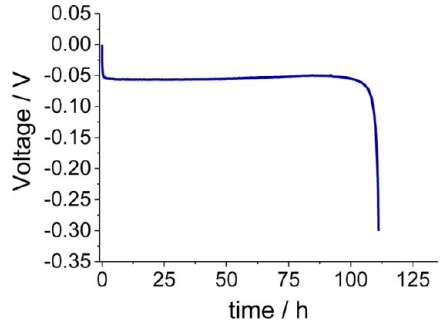

Figure 6. Voltage profile behavior of a Li/Li pouch cell during galvanostatic plating. T = 40 °C, i = 0.1 mA cm^{-2}.

throughout deposition, indicating that the concentration gradient has reached a steady state. However, soon after the total capacity of the working electrode has been plated, a steep increase in ΔV indicates that Li^+ depletion occurs.

Different pouch cells were stopped at different plating/stripping stages (30, 60, and 90%) and SEM images of their electrodes were taken to observe morphological changes (Figure 7).

The striped features observed on the pristine sample remained unchanged after every step of the process, on both the pin-striped and plated electrodes. This important finding denotes the good compatibility between Li metal and ionic liquid electrolytes, especially in terms of the stable SEI that does not suffer from cracking during long-term, continuous plating (ca. 100 h).

The fact that the aspect ratio of the stripped features does not change, either during Li dissolution or deposition, indicates that the SEI formed is a homogeneous ionic conductor with no defects, and that, below i_{lim}, no favored regions for Li^+ transport arise over time. Most likely, the SEI's favorable properties

DOI: 10.1021/acsami.5b00209
ACS Appl. Mater. Interfaces 2015, 7, 5950–5958

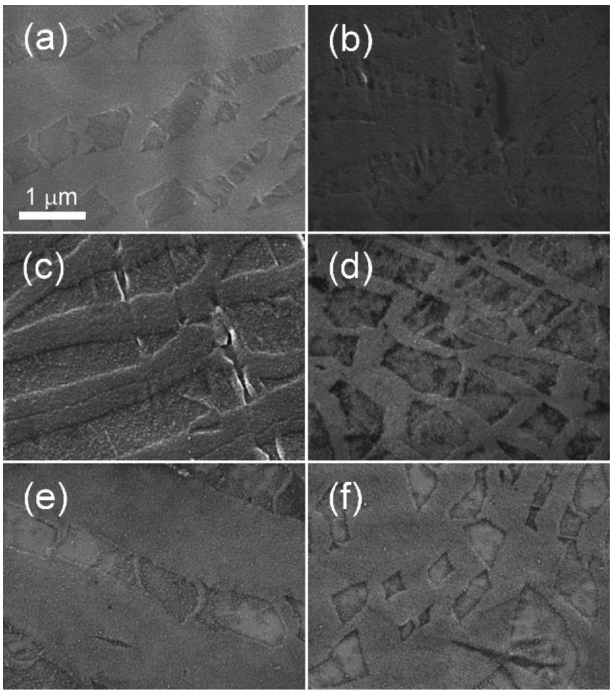

Figure 7. Surface of cycled Li electrodes after cycling (a and b) 30, (c and d) 60, and (e and f) 90%. Images on the left are of the plated side, and images on the right are of the pin-striped side.

originate from the storage of our Li foil in a dry room for long periods of time, where reactivity with moisture is limited. Other components of the atmosphere (such as CO_2) can, however, still react with the foil, leading to the slow accumulation of an inorganic Li_2CO_3 layer that is homogeneous over the whole surface, as the XPS measurements depicted in Figure 8 show.

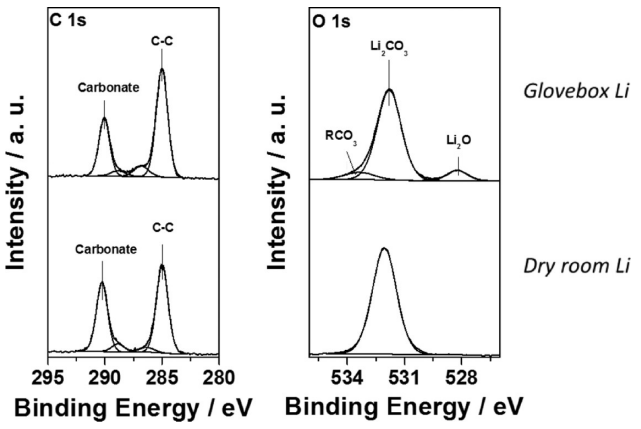

Figure 8. X-ray photoelectron spectra performed on two types of pristine Li foil: (left) C 1s peaks and (right) O 1s peaks.

Li foil that is stored in a dry room has a surface content of Li_2CO_3 that is 38% higher than lithium normally stored under an Ar atmosphere. Also, Li_2O was not found on the surface of the dry room lithium, which is consistent with other reports showing that it is located underneath lithium carbonate.[43,44] The O 1s peak related to Li_2O was, however, detected in the case of the thicker lithium stored in an Ar-filled glovebox, suggesting that in this case the carbonate layer could be inhomogeneous, thin enough to allow the detection of the primary SEI, or both. Lithium carbonate has already shown a positive influence on lithium by lowering the electrodes' polarization and the interfacial resistance.[45] CO_2, which is a common constituent of atmospheric air, can effectively react with Li_2O and build a thick layer of Li_2CO_3, a compound that has the remarkable property of providing fast intermolecular Li^+ exchange.[46−48] Because poor deposition is driven by impurities and lattice defects, this brings us to the conclusion that either our pouch cells contain very pure chemicals or that the SEI we were able to form on lithium has the power to suppress their effects. Upon the secondary SEI and between the grain boundaries, a plastic, organic matrix also forms, originating from the IL electrolyte. This SEI composition, which is largely agreed upon, is particularly stable under the conditions described in this study. Finally, although no dendrites were observed on the 30−90% samples, we did note interesting features on a fully plated electrode. Figure 9a gives an overview of the general appearance of the 100% plated electrode, which does not differ much from the ones depicted in Figure 5a−f. However, dramatic changes in morphology were found in some areas of the Li electrode. As seen in Figure 9b, a landscape made of plateaus several micrometers wide between separator fibers hints to an extrusion process taking place on the surface, in good accordance with Yamaki's model,[9] despite the notable difference in size between these structures and common dendrites. Figure 9c illustrates the rupture of the Li surface on one of such plateaus, with fibrous features filling the gap between the two Li "plates". These fibers of ca. 50−100 nm, identical in size to the discrete deposits on Ni recorded in Figures 1a and 3a−c, are densely packed into bundles, which suggests that the deposition of Li below the SEI occurs under this form prior to cracking. Additionally, the upper plate deforms into an arched shape, indicating a preferential deposition caused by local changes in Li^+ concentration. The formation of "scars" on the arched surface is an indication of the significant stress exerted onto the SEI surface under localized Li deposition and the self-repair mechanism that is triggered once fresh Li is exposed to the electrolyte. Zooming into the fracture gives more insight into what happens on this freshly created surface. In Figure 9d, it is possible to see a series of 50 nm-wide nucleation sites along the fiber bundles. These globular features only grow up to a few nanometers before reaching a halt, probably because of a rapid SEI formation; another site on the same crack (Figure 9e) shows the presence of lozenge-shaped terraces that give rise to "steps" with different heights. This confirms the intensive stress the SEI is subjected to and the crystalline nature of the products of which it is composed. Finally, it is noteworthy to make a comparison between our findings and what was recently observed by Cui et al.[22] (Figure 9f), who deposited Li underneath a nanostructured carbon shell; in their study, they also grow Li in a fibrous fashion with micrometer-sized bundles that closely resemble those observed in the SEI cracks (Figure 9c−e).

A close look at the protuberances in Figure 10a, which are most likely a further evolution of the cracks, shows that new Li surface is created during extrusion, pushing the old surface aside together with the previously deposited Li. Figure 10b,c summarizes the growth mechanism we propose for the formation of such protuberances. According to our interpretation, the deposition of Li takes place uniformly, below the SEI, under the form of densely packed nanofibers as long as the supply of Li^+ ions is homogeneous over the whole electrode. Once the Li at the counter electrode and in solution is close to depletion, local inhomogeneities arise as a result of the small Li reservoirs (Li islands) remaining on the stripped electrode, favoring deposition at specific sites and exerting strain on the SEI.

DOI: 10.1021/acsami.5b00209
ACS Appl. Mater. Interfaces 2015, 7, 5950−5958

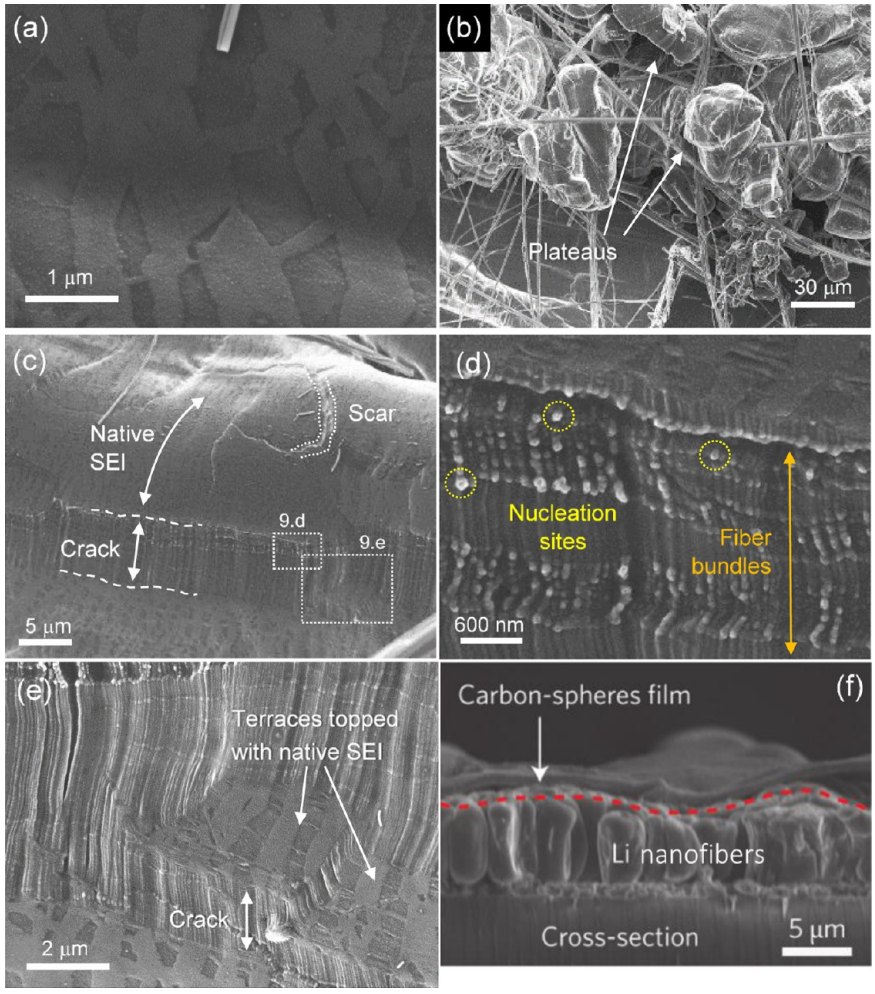

Figure 9. (a) Overview of a fully plated Li electrode; (b) area affected by inhomogeneous plating; (c) rupture in the SEI resulting from inhomogeneous plating; (d) magnification of the fiber-like features observed in the crack; (e) SEI terraces; (f) fibrous Li deposits as shown by Cui et al.[22] Reproduced with permission of the Nature Publishing Group, 2014.

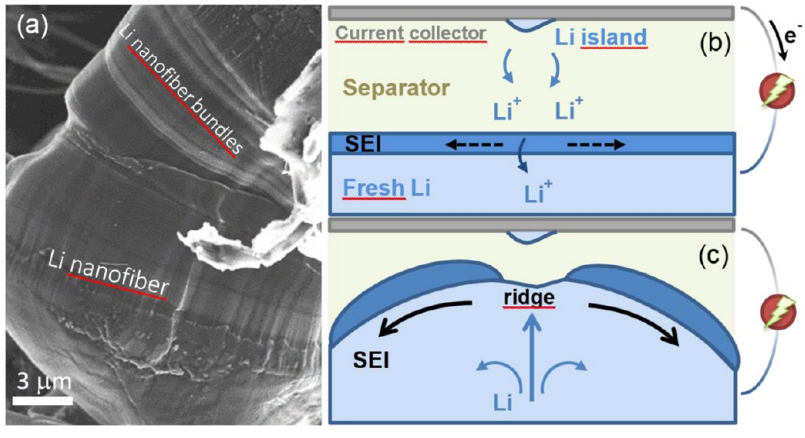

Figure 10. (a) Li nanofibers bundles extruded from the native SEI; (b and c) SEI rupture mechanism resulting from the local variations of Li^+ concentration outside of a steady-state regime.

The resulting forces lead to the unzipping of the surface, first exposing the Li fibers and the subsequent extrusion of fresh Li in what resembles a ridge, as seen in Figure 10a, and then creating new Li surface, which pushes both the native SEI and the previously deposited fibrous lithium out of the plane. The freshly exposed surface does not lead to dendrite growth (nor favored Li deposition, as suggested by the concave shape inside the ridge), which could be due to the rapid formation of a favorable SEI or, on the contrary, an SEI that does not allow nucleation. This extrusion mechanism differs from Yamaki et al.'s description,[9] as the SEI is deformed and no dendrite whiskers form.

DOI: 10.1021/acsami.5b00209
ACS Appl. Mater. Interfaces 2015, 7, 5950−5958

4. CONCLUSIONS

In summary, we have confirmed that the FSI^- anion in ionic liquid-based electrolytes has a beneficial influence over the SEI on lithium metal, especially compared to $TFSI^-$, thanks to its slightly inferior electrochemical cathodic stability. The presence of the more stable $TFSI^-$ anion hinders traditional Li/Ni plating/stripping tests, most likely because no nucleation-favorable film forms on nickel. The result is a nonuniform Li deposition, which might be improved with the addition of the FSI^- anion. An alternative route to Li/Ni efficiency determination tests has been therefore devised, which not only allows these tests to be performed, but also shows that $Pyr_{14}TFSI$-based electrolytes enable a uniform Li deposition/dissolution and high cycling efficiencies, with no signs of dendrite formation. Our observations show that $Pyr_{14}TFSI$-based electrolytes, under the right conditions, allow a homogeneous Li^+ deposition, as shown through scanning electron microscopy. Finally, we observed interesting surface features while operating the cell under a Li^+ depletion regime. Large micrometer-sized plateaus appear because of local variations in Li^+ concentration, with fibrous Li bundles extruding out of ruptures in the SEI texture. The formation of whisker-like dendrites on these freshly exposed surfaces is inhibited by the rapid evolution of a solid-electrolyte interphase in what can be seen as an efficient self-repair mechanism. The lack of dendrites and whiskers in our system indicates that ionic liquid electrolytes are apt for safe use in lithium metal batteries in relation to conventional electrolytes. Finally, the reduced Li loss is a promising finding that will ultimately help building batteries with a reduced excess Li on the anode, thus attaining higher practical gravimetric and volumetric energy densities.

AUTHOR INFORMATION

Corresponding Authors

*E-mail: elie.paillard@kit.edu.

*E-mail: stefano.passerini@kit.edu.

Author Contributions

The manuscript was written through contributions of all authors. All authors have given approval to the final version of the manuscript.

Notes

The authors declare no competing financial interest.

ACKNOWLEDGMENTS

L.G, E.P., and S.P. would like to acknowledge the support of the European Commission FP7 Project "Lithium−Air Battery with Split Oxygen Harvesting and Redox Processes" (LABOHR) (FP7-NMP-2010, grant agreement No. 265971) and the Project "Stable Interfaces for Rechargeable Batteries" (SIRBATT) (FP7-ENERGY-2013, grant agreement No. 608502).

REFERENCES

(1) Scrosati, B. Lithium Rocking Chair Batteries: An Old Concept? *J. Electrochem. Soc.* **1992**, *139*, 2776−2781.

(2) Bruce, P. G.; Freunberger, S. A.; Hardwick, L. J.; Tarascon, J.-M. $Li-O_2$ and Li−S Batteries with High Energy Storage. *Nat. Mater.* **2011**, *11*, 19−29.

(3) Fergus, J. W. Recent Developments in Cathode Materials for Lithium Ion Batteries. *J. Power Sources* **2010**, *195*, 939−954.

(4) Peled, E. The Electrochemical Behavior of Alkali and Alkaline Earth Metals in Nonaqueous Battery Systems—the Solid Electrolyte Interphase Model. *J. Electrochem. Soc.* **1979**, 2047−2051.

(5) Rosso, M.; Brissot, C.; Teyssot, A.; Dollé, M.; Sannier, L.; Tarascon, J.-M.; Bouchet, R.; Lascaud, S.; Dollé, M. Dendrite Short-Circuit and Fuse Effect on Li/polymer/Li Cells. *Electrochim. Acta* **2006**, *51*, 5334−5340.

(6) Chazalviel, J.-N. Electrochemical Aspects of the Generation of Ramified Metallic Electrodeposits. *Phys. Rev. A* **1990**, *42*, 7355−7367.

(7) Rosso, M.; Gobron, T.; Brissot, C.; Chazalviel, J. N.; Lascaud, S. Onset of Dendritic Growth in Lithium/polymer Cells. *J. Power Sources* **2001**, *97*−*98*, 804−806.

(8) Rosso, M.; Chassaing, E.; Chazalviel, J.-N.; Gobron, T. Onset of Current-Driven Concentration Instabilities in Thin Cell Electrodeposition with Small Inter-Electrode Distance. *Electrochim. Acta* **2002**, *47*, 1267−1273.

(9) Yamaki, J.; Tobishima, S.; Hayashi, K.; Nemoto, Y.; Arakawa, M. A Consideration of the Morphology of Electrochemically Deposited Lithium in an Organic Electrolyte. *J. Power Sources* **1998**, *74*, 219−227.

(10) Brissot, C.; Rosso, M.; Chazalviel, J. N.; Lascaud, S. Dendritic Growth Mechanisms in Lithium/polymer Cells. *J. Power Sources* **1999**, 925−929.

(11) Gireaud, L.; Grugeon, S.; Laruelle, S.; Yrieix, B.; Tarascon, J.-M. Lithium Metal Stripping/plating Mechanisms Studies: A Metallurgical Approach. *Electrochem. Commun.* **2006**, *8*, 1639−1649.

(12) Mayers, M. Z.; Kaminski, J. W.; Miller, T. F. Suppression of Dendrite Formation via Pulse Charging in Rechargeable Lithium Metal Batteries. *J. Phys. Chem. C* **2012**, *116*, 26214−26221.

(13) Kim, S.-H.; Choi, K.-H.; Cho, S.-J.; Kil, E.-H.; Lee, S.-Y. Mechanically Compliant and Lithium Dendrite Growth-Suppressing Composite Polymer Electrolytes for Flexible Lithium-Ion Batteries. *J. Mater. Chem. A* **2013**, *1*, 4949.

(14) Schweikert, N.; Hofmann, A.; Schulz, M.; Scheuermann, M.; Boles, S. T.; Hanemann, T.; Hahn, H.; Indris, S. Suppressed Lithium Dendrite Growth in Lithium Batteries Using Ionic Liquid Electrolytes: Investigation by Electrochemical Impedance Spectroscopy, Scanning Electron Microscopy, and in Situ 7Li Nuclear Magnetic Resonance Spectroscopy. *J. Power Sources* **2013**, *228*, 237−243.

(15) Best, A. S.; Bhatt, A. I.; Hollenkamp, A. F. Ionic Liquids with the Bis(fluorosulfonyl)imide Anion: Electrochemical Properties and Applications in Battery Technology. *J. Electrochem. Soc.* **2010**, *157*, A903.

(16) Min, S.; Su, I.; Sun, Y.; Song, J.-H.; Chung, S.; Kim, D.; Choi, S. M.; Kang, I. S. Cycling Characteristics of Lithium Metal Batteries Assembled with a Surface Modified Lithium Electrode. *J. Power Sources* **2013**, *244*, 363−368.

(17) Ding, F.; Xu, W.; Graff, G. L.; Zhang, J. J.-G.; Sushko, M. L.; Chen, X.; Shao, Y.; Engelhard, M. H.; Nie, Z.; Xiao, J.; Liu, X.; Sushko, P. V.; Liu, J.; Zhang, J.-G. Dendrite-Free Lithium Deposition via Self-Healing Electrostatic Shield Mechanism. *J. Am. Chem. Soc.* **2013**, *135*, 4450−4456.

(18) Ding, F.; Xu, W.; Chen, X.; Zhang, J.; Shao, Y.; Engelhard, M. H.; Zhang, Y.; Blake, T. a; Graff, G. L.; Liu, X.; Zhang, J.-G. Effects of Cesium Cations in Lithium Deposition via Self-Healing Electrostatic Shield Mechanism. *J. Phys. Chem. C* **2014**, *118*, 4043−4049.

(19) Sano, H.; Sakaebe, H.; Matsumoto, H. In-Situ Optical Microscope Morphology Observation of Lithium Electrodeposited in Room Temperature Ionic Liquids Containing Aliphatic Quaternary Ammonium Cation. *Electrochemistry* **2012**, 777−779.

(20) Basile, A.; Bhatt, A. I.; O'Mullane, A. A Combined Scanning Electron Micrograph and Electrochemical Study of the Effect of Chemical Interaction on the Cyclability of Lithium Electrodes in an Ionic Liquid. *Aust. J. Chem.* **2012**, 9−10.

(21) Kim, H.; Jeong, G.; Kim, Y.-U.; Kim, J.-H.; Park, C.-M.; Sohn, H.-J. Metallic Anodes for next Generation Secondary Batteries. *Chem. Soc. Rev.* **2013**, *42*, 9011−9034.

(22) Zheng, G.; Lee, S. W.; Liang, Z.; Lee, H.-W.; Yan, K.; Yao, H.; Wang, H.; Li, W.; Chu, S.; Cui, Y. Interconnected Hollow Carbon Nanospheres for Stable Lithium Metal Anodes. *Nat. Nanotechnol.* **2014**, 1−6.

(23) Monroe, C.; Newman, J. Dendrite Growth in Lithium/Polymer Systems−A Propagation Model for Liquid Electrolytes under Galvanostatic Conditions. *J. Electrochem. Soc.* **2003**, *150*, A1377.

DOI: 10.1021/acsami.5b00209
ACS Appl. Mater. Interfaces 2015, 7, 5950−5958

(24) Steiger, J.; Kramer, D.; Mönig, R. Mechanisms of Dendritic Growth Investigated by in Situ Light Microscopy during Electrodeposition and Dissolution of Lithium. *J. Power Sources* **2014**, *261*, 112−119.
(25) Steiger, J.; Kramer, D.; Mönig, R. Microscopic Observations of the Formation, Growth and Shrinkage of Lithium Moss during Electrodeposition and Dissolution. *Electrochim. Acta* **2014**, *136*, 529−536.
(26) Harry, K. J.; Hallinan, D. T.; Parkinson, D. Y.; MacDowell, A. a.; Balsara, N. P. Detection of Subsurface Structures underneath Dendrites Formed on Cycled Lithium Metal Electrodes. *Nat. Mater.* **2013**, *12*, 1−6.
(27) Nishida, T.; Nishikawa, K.; Rosso, M.; Fukunaka, Y. Optical Observation of Li Dendrite Growth in Ionic Liquid. *Electrochim. Acta* **2013**, *100*, 333−341.
(28) Li, Z.; Huang, J.; Yann Liaw, B.; Metzler, V.; Zhang, J. A Review of Lithium Deposition in Lithium-Ion and Lithium Metal Secondary Batteries. *J. Power Sources* **2014**, *254*, 168−182.
(29) Basile, A.; Hollenkamp, A. F.; Bhatt, A. I.; O'Mullane, A. P. Extensive Charge−Discharge Cycling of Lithium Metal Electrodes Achieved Using Ionic Liquid Electrolytes. *Electrochem. commun* **2013**, *27*, 69−72.
(30) Philippe, B.; Dedryvère, R.; Gorgoi, M.; Rensmo, H.; Gonbeau, D.; Edström, K. Improved Performances of Nanosilicon Electrodes Using the Salt LiFSI: A Photoelectron Spectroscopy Study. *J. Am. Chem. Soc.* **2013**, *135*, 9829−9842.
(31) Eshetu, G. G.; Grugeon, S.; Gachot, G.; Mathiron, D.; Armand, M.; Laruelle, S. LiFSI vs. LiPF6 Electrolytes in Contact with Lithiated Graphite: Comparing Thermal Stabilities and Identification of Specific SEI-Reinforcing Additives. *Electrochim. Acta* **2013**, *102*, 133−141.
(32) Grande, L.; Paillard, E.; Kim, G.; Passerini, S. Ionic Liquid Electrolytes for Li−Air Batteries: Lithium Metal Cycling. *Int. J. Mol. Sci.* **2014**, *15*, 8122−8137.
(33) Randström, S.; Appetecchi, G. B.; Lagergren, C.; Moreno, A.; Passerini, S. The Influence of Air and Its Components on the Cathodic Stability of *N*-Butyl-*N*-methylpyrrolidinium Bis-(trifluoromethanesulfonyl)imide. *Electrochim. Acta* **2007**, *53*, 1837−1842.
(34) Randström, S.; Montanino, M.; Appetecchi, G. B.; Lagergren, C.; Moreno, A.; Passerini, S. Effect of Water and Oxygen Traces on the Cathodic Stability of *N*-Alkyl-*N*-methylpyrrolidinium Bis-(trifluoromethanesulfonyl)imide. *Electrochim. Acta* **2008**, *53*, 6397−6401.
(35) Appetecchi, G. B.; Scaccia, S.; Tizzani, C.; Alessandrini, F.; Passerini, S. Synthesis of Hydrophobic Ionic Liquids for Electrochemical Applications. *J. Electrochem. Soc.* **2006**, *153*, A1685−A1691.
(36) Kim, G.; Appetecchi, G. B.; Montanino, M. Long-Term Cyclability of Lithium Metal Electrodes in Ionic Liquid-Based Electrolytes at Room Temperature. *ECS Trans.* **2010**, *25*, 127−138.
(37) Howlett, P. C.; Macfarlane, D. R.; Hollenkamp, A. F. High Lithium Metal Cycling Efficiency in a Room-Temperature Ionic Liquid. *Electrochem. Solid-State Lett.* **2004**, *7*, A97.
(38) Wibowo, R. Ionic Liquid *N*-Butyl-*N*-Methylpyrrolidinium Bis(trifluoromethylsulfonyl) Imide in the Temperature Range 298−318 K: A Theoretical and Experimental Study Using Pt. *J. Phys. Chem. B* **2009**, 12293−12298.
(39) Ishikawa, M.; Sugimoto, T.; Kikuta, M.; Ishiko, E.; Kono, M. Pure Ionic Liquid Electrolytes Compatible with a Graphitized Carbon Negative Electrode in Rechargeable Lithium-Ion Batteries. *J. Power Sources* **2006**, *162*, 658−662.
(40) Paillard, E.; Zhou, Q.; Henderson, W. A.; Appetecchi, G. B.; Montanino, M.; Passerini, S. Electrochemical and Physicochemical Properties of $PY_{14}FSI$-Based Electrolytes with LiFSI. *J. Electrochem. Soc.* **2009**, *156*, A891.
(41) Appetecchi, G. B.; Montanino, M.; Balducci, A.; Lux, S. F.; Winter, M.; Passerini, S. Lithium Insertion in Graphite from Ternary Ionic Liquid-Lithium Salt Electrolytes I. Electrochemical Characterization of the Electrolytes. *J. Power Sources* **2009**, *192*, 599−605.
(42) Kunze, M.; Jeong, S.; Appetecchi, G. B.; Schönhoff, M.; Winter, M.; Passerini, S. Mixtures of Ionic Liquids for Low Temperature Electrolytes. *Electrochim. Acta* **2012**, *82*, 69−74.
(43) Ismail, I.; Noda, A.; Nishimoto, A.; Watanabe, M. XPS Study of Lithium Surface after Contact with Lithium-Salt Doped Polymer Electrolytes. *Electrochim. Acta* **2001**, *46*, 1595−1603.
(44) Kanamura, K.; Shiraishi, S.; Tamura, H.; Takehara, Z. X-Ray Photoelectron Spectroscopic Analysis and Scanning Electron Microscopic Observation of the Lithium Surface Immersed in Nonaqueous Solvents. *J. Electrochem. Soc.* **1994**, *141*, 2379−2385.
(45) Chung, K.; Lee, J.-D.; Kim, E.-J.; Kim, W.-S.; Cho, J.-H.; Choi, Y.-K. Studies on the Effects of Coated Li_2CO_3 on Lithium Electrode. *Microchem. J.* **2003**, *75*, 71−77.
(46) Gan, H.; Takeuchi, E. S. Lithium Electrodes with and without CO_2 Treatment: Electrochemical Behavior and Effect on High Rate Lithium Battery Performance. *J. Power Sources* **1996**, *62*, 45−50.
(47) Iddir, H.; Curtiss, L. Li Ion Diffusion Mechanisms in Bulk Monoclinic Li_2CO_3 Crystals from Density Functional Studies. *J. Phys. Chem. C* **2010**, *114*, 20903−20906.
(48) Shang, S.-L.; Hector, L. G.; Shi, S.; Qi, Y.; Wang, Y.; Liu, Z.-K. Lattice Dynamics, Thermodynamics and Elastic Properties of Monoclinic Li_2CO_3 from Density Functional Theory. *Acta Mater.* **2012**, *60*, 5204−5216.

DOI: 10.1021/acsami.5b00209
ACS Appl. Mater. Interfaces 2015, 7, 5950−5958